Energy Engineering

Tech Science Press

Doi:10.32604/ee.2025.061083

ARTICLE

Correlation Analysis of Power Quality and Power Spectrum in Wind Power Hybrid Energy Storage Systems

Jian Gao[1], Hongliang Hao[2], Caifeng Wen[1,*], Yongsheng Wang[3], Zhanhua Han[4], Edwin E. Nykilla[2] and Yuwen Zhang[2]

[1]College of Energy and Power Engineering, Inner Mongolia University of Technology, Hohhot, 010051, China
[2]Ordos Energy Research Institute, Peking University, Ordos City, 017000, China
[3]School of Data Science and Application, Inner Mongolia University of Technology, Hohhot, 010051, China
[4]Inner Mongolia Baotou Steel Pipe Co., Ltd., Baotou City, 014010, China

*Corresponding Author: Caifeng Wen. Email: wencfg@imut.edu.cn

Received: 16 November 2024; Accepted: 16 January 2025; Published: 07 March 2025

ABSTRACT: Power quality is a crucial area of research in contemporary power systems, particularly given the rapid proliferation of intermittent renewable energy sources such as wind power. This study investigated the relationships between power quality indices of system output and PSD by utilizing theories related to spectra, PSD, and random signal power spectra. The relationship was derived, validated through experiments and simulations, and subsequently applied to multi-objective optimization. Various optimization algorithms were compared to achieve optimal system power quality. The findings revealed that the relationships between power quality indices and PSD were influenced by variations in the order of the power spectral estimation model. An increase in the order of the AR model resulted in a 36% improvement in the number of optimal solutions. Regarding optimal solution distribution, NSGA-II demonstrated superior diversity, while MOEA/D exhibited better convergence. However, practical applications showed that while MOEA/D had higher convergence, NSGA-II produced superior optimal solutions, achieving the best power quality indices (THDi at 4.62%, d% at 3.51%, and cos φ at 96%). These results suggest that the proposed method holds significant potential for optimizing power quality in practical applications.

KEYWORDS: Wind power generation; hybrid energy storage; power quality; PSD; NSGA-II

1 Introduction

As global energy demand and environmental concerns escalate, developing renewable and clean energy sources has emerged as a crucial direction for global energy transformation. Solar, wind, and hydroelectric power are gradually becoming the primary alternatives to traditional fossil fuels due to their environmental sustainability and other advantages. For instance, the integrated optimization of solar and gas turbine systems can substantially enhance energy efficiency while reducing emissions [1]. Solid oxide fuel cell systems demonstrate excellent power output and low emissions across various current densities [2]. Furthermore, the combination of biomass gasification and solid oxide fuel cells has the potential to improve system energy efficiency [3]. Innovative approaches to converting waste into renewable hydrogen also provide new ideas for clean energy production [4]. Compared to other clean energy sources, integrating wind energy into power systems significantly reduces generation costs and emissions [5] and enhances system scheduling efficiency. Research indicates that wind energy integration demonstrates notable advantages in multi-objective optimization, particularly in large-scale power systems [6].

Many comparative analyses of accuracy and flexibility characteristics in the frequency domain through Fourier transform methods have recently been proposed [7]. Power spectrum analysis based on Fourier transform is extensively utilized across various fields [8,9]. For instance, Leonowicz et al. [10] evaluated power quality using an advanced spectrum approach and found that higher-resolution spectra improved the accuracy of assessed spectral parameters in deformed power system waveforms. Similarly, Wang et al. [11] investigated power quality disruption characteristics using deep learning, achieving a satisfactory accuracy of 98.43% in power evaluation. Narendra Babu [12] conducted an adaptive grid mentor control test for power quality in a microgrid system, demonstrating promising results with direct current (DC) usage in microgrids. Shao et al. [13] reviewed power quality monitoring in offshore wind energy, identifying synchronized waveform detection as having great potential due to its high resolution, availability, and effective time synchronization. Holdynski et al. [14] analyzed the impact of photovoltaic farms on select power quality parameters in medium power grids, observing a 60% decrease in voltage distortion factor with increased power. Tian [15] employed PSD and autocorrelation function analyses to explore chaotic dynamic behavior in wind-electric time series at various time scales. Yao et al. [16] applied the hinge model in PSD analysis to obtain low-pass decomposition frequency, achieving an optimized energy storage scale for single-day energy balance. Qing et al. [17] utilized PSD to capture the frequency and amplitude of state variable fluctuations in heterogeneous power systems with random excitation. Ayon et al. [18] estimated the coherence index from self-PSD and cross-PSD information to identify coherent regions of specific frequencies associated with interregional oscillation patterns. In optimization systems, Morteza et al. [19] proposed a distribution network development and planning model based on electric vehicles and distributed power sources, analyzing electric vehicles' influence on the technical characteristics of power grids in intelligent environments through scenario simulations. Reference [20] employed the Antlion optimization algorithm to optimize parameters of model predictive control (MPC) and proportional-integral (PI) controllers, adjusting plug-in hybrid electric vehicle (PHEV) battery charging rates to reduce frequency fluctuations caused by wind energy variations.

Power quality is a crucial indicator for assessing the stability and reliability of a power system. Karafotis et al. [21] introduced a wavelet packet transform-based method for power quality analysis in three-phase power systems, considering harmonics and unbalance. Yin et al. [22] evaluated the overall power quality of new energy permeation distribution network systems using the analytic hierarchy process (AHP). Total harmonic distortion (THD), a significant index, is frequently utilized in power quality studies. Higher THD values indicate poorer power quality, potentially leading to issues such as reduced equipment lifespan, increased system losses, and equipment malfunctions. Reference [23] proposed an artificial neural network (ANN)-based excitation current modulation method, which effectively mitigated terminal voltage harmonic distortion in synchronous generators under nonlinear load conditions by optimizing the excitation current. Reference [24] presented a novel multilevel alternating current (AC)/DC/AC multiunit converter topology that significantly reduced THD in wind energy conversion systems and enhanced the voltage output quality of grid-connected wind energy systems.

Despite the prevalence of PSD analysis in various fields, its application in conjunction with power quality indices to examine wind power hybrid energy storage systems remains limited. This study primarily investigates the output power quality of wind power hybrid energy storage systems. Additionally, it explores the relationship between PSD and power quality indices through theoretical derivation of random signal power spectra, which is supported by experimental and simulation verification. Through comprehensive multi-objective optimization comparisons, this research achieves an optimal state of power quality, providing an effective and reliable framework for evaluating and enhancing the output power quality of wind power systems.

2 Related Theory and System Power Spectrum Calculation

2.1 FFT to PSD Conversion

Random signals lack the property of Fourier transform, resulting in theoretically infinite total energy when calculated. To apply Fourier transform methods to random signals, energy spectrum calculation involves using an interceptor function. Subsequently, the power spectrum of random signals is derived by linking spectrum analysis with random signals through Parseval's theorem. Consider a discretized sample x(n) of the random process X(t), with a finite length N and a sampling interval of $\triangle t$, where $\triangle t$ can be treated as a finite energy sequence. If the discrete-time Fourier transform $x_N\left(e^{jw}\right)$ of $x_N\left(n\right)$ exists, then based on the relationship between discrete-time Fourier transform and Fourier transform [25], the PSD of the discrete-time random sequence can be derived as shown in Eq. (1):

$$G_X\left(f\right) = \frac{1}{N}\left|\sum_{1}^{N} x_n\left(t\right) e^{-j2\pi f n\Delta t}\Delta t\right|^2 \tag{1}$$

According to the calculation method provided by Matlab, the conversion relationship between PSD and spectrum can be obtained through Eq. (2):

$$PSD\left(x\right) = 2\left(\frac{1}{Fs \cdot N}\right)\left|x\right|^2 \tag{2}$$

where Fs represents the sampling frequency, and $|x|$ denotes the amplitude after discrete Fourier transform.

2.2 Mathematical Derivation of System PSD and Power Quality Indices

The subsequent section presents mathematical calculations for the power spectrum and power quality indices of the system. Initially, a mathematical model and corresponding complex domain are established based on the power spectrum concept. This is followed by an examination of the nonlinear characteristics of system components, including the aerodynamic properties of wind turbines and the switching characteristics of electronic control devices. To simplify the analysis, a linearization method is employed to approximate the nonlinear system near a specific operating point, yielding a linear system through frequency deviation.

Frequency deviation:

The PSD can be computed by multiplying the signal's Fourier transform in the frequency domain with its complex conjugate and averaging the result. Using this method, the PSD of wind fluctuation is calculated [25], and its formula is expressed as follows:

$$S_w\left(f\right) = \frac{1}{\Delta f}\frac{1}{n}\sum_{i=1}^{n} X_i\left(f\right) X_i^*\left(f\right) \tag{3}$$

where Δf represents the sampling frequency.

Through the application of random signal analysis and frequency-domain analysis of the linear system, the relationship between the input signal $S_w\left(f\right)$ and the PSD $S_y\left(f\right)$ of the system's output signal is expressed by the following formula:

$$S_y\left(f\right) = \left|H\left(f\right)\right|^2 S_w\left(f\right) \tag{4}$$

Assuming the input signal x(t) is a zero-mean stochastic stationary process, the PSD corresponding to the variance of the output y(t) can be obtained as

$$\sigma_y^2 = \frac{1}{2\pi} \int_{-\infty}^{\infty} S_y(f)\, df \tag{5}$$

Disregarding the generator governor, the model transfer function of the system frequency characteristic is expressed as

$$G(s) = \frac{1}{2Ts + \beta} \tag{6}$$

where T denotes the inertia constant of system time, and β represents the load-frequency characteristic coefficient.

Moreover, the study calculates the impact of the synchronous generator and energy storage device when wind power fluctuation $\chi_{pw}(s)$ results in frequency deviation $\chi_f(s)$ following the system frequency response. This relationship is expressed by

$$\chi_f(s) = [G(s) - P_G(s) - P_B(s)]\, \chi_{pw}(s) \tag{7}$$

where $P_G(s)$ and $P_B(s)$ represent the transfer functions of the synchronous generator and the energy storage device, respectively.

The corresponding input signal $S_y(f)$ of the system can be derived from Eq. (4) and expressed as

$$S_y(f) = |G(s) - P_G(s) - P_B(s)|^2 \cdot S_w(f) \tag{8}$$

Upon substitution of $S_y(f)$ into Eq. (5), the variance of the system frequency deviation PSD can be expressed as

$$\sigma_f^2 = \frac{1}{2\pi} \int_{-\infty}^{\infty} |G(s) - P_G(s) - P_B(s)|^2 \cdot S_w(f)\, df \tag{9}$$

Additional power quality indices are associated with the power spectrum through the spectrum from Eq. (2), and THDi can be simply expressed by

$$THDi = \sqrt{\frac{\sum_{n=2}^{\infty} I_n^2}{I_1^2}} \tag{10}$$

By multiplying the numerator and denominator of Eqs. (2) and (10), the relationship between THDi and PSD can be expressed as

$$THDi = \sqrt{\frac{\sum_{n=2}^{\infty} PSD(I_n)}{PSD(I_1)}} \tag{11}$$

where I_1 represents the RMS value of the fundamental current, and I_n denotes the RMS value of the n-th harmonic current.

The power factor ($\cos\varphi$) can be expressed by its relationship with the harmonics of the rectifier circuit. In a public power grid, this occurs when voltage waveform distortion is minimal and current waveform distortion is substantial. According to Reference [26], voltage distortion can be disregarded, and the power factor can be expressed as

$$\cos\varphi = \frac{P}{S} = \frac{UI_1\cos\varphi_1}{UI} = \frac{I_1}{I}\cos\varphi_1 \tag{12}$$

The relationship between $\cos\varphi$ and PSD can be expressed through Eq. (1) as follows:

$$\cos\varphi = \frac{PSD\left(I_1\right)}{PSD\left(I\right)}\cos\varphi_1 \tag{13}$$

In the case of non-sinusoidal reactive power $Q_f = UI_1\sin\varphi_1$ and $S^2 \neq P^2 + Q_f^2$, the distortion power D is derived as follows:

$$\begin{aligned} &S^2 = P^2 + Q_f^2 + D^2 \\ &D = U\sqrt{\sum_{n=2}^{\infty} I_n^2} \Rightarrow D\cdot\sqrt{\frac{2}{Fs\cdot N}} = \sqrt{\sum_{n=2}^{\infty} PSD\left(I_n\right)} \end{aligned} \tag{14}$$

where I represents the effective value of distortion current, and $\cos\varphi_1$ denotes the fundamental power factor.

Establish a signal model formula comprising a fundamental frequency component and a single interharmonic component as follows:

$$u\left(t\right) = V_i\left[\sin\left(2\pi f_i t\right) + m\sin\left(2\pi f_{iH} t + \theta_{iH}\right)\right] \tag{15}$$

where V_i, f_i, m, f_{iH}, and θ_{iH} denote the peak value of fundamental frequency, fundamental frequency, relative amplitude of interharmonic, interharmonic frequency, and phase angle, respectively.

By setting $f_{iH} = hf_i + \Delta f_h$, where h represents the number of harmonics closest to f_{iH}, and assuming the interharmonic phase angle θ_{iH} is zero, the voltage expansion formula is given by Eq. (16):

$$u\left(t\right) = V_i\left[\sin\left(2\pi f_i t\right) + m\cos\left(2\pi\Delta f_h t\right)\right]\sin\left(2\pi h f_i t\right) + V_i m\sin\left(2\pi\Delta f_h t\right)\cos\left(2\pi h f_i t\right) \tag{16}$$

An analysis of the expansion above reveals that the waveform incorporates a harmonic component hf_i with an amplitude variation of $V_i m\sin\left(2\pi\Delta f_h t\right)$. By the definition of the effective value of voltage fluctuation [27], the formula for d_{RMS} is derived and presented as in Eq. (17):

$$\begin{aligned} &d_{RMS} = \left.\frac{\Delta U}{U_N}\right|_{RMS} = \frac{U_{RMS-\max} - U_{RMS-\min}}{U_N}\times 100\% \\ &\approx \left|\frac{2m}{1+\Delta f_i\cdot T_0/2}\cdot\frac{\sin\left(\pi\Delta f_i\cdot T_0\right)}{\pi\Delta f_i\cdot T_0}\right| \end{aligned} \tag{17}$$

The analysis reveals that the deviation between the interharmonic and fundamental frequencies (Δf_i) and the relative amplitude of the interharmonic (m_{ih}) exhibit fluctuations proportional to the root value of the voltage square. A direct correlation exists between their magnitudes d_{RMS}, as described by Reference [27] and expressed in Eq. (18) below:

$$m = \frac{V_n}{V_1}\times 100\% = \frac{PSD\left(V_n\right)}{PSD\left(V_1\right)}\times 100\% \tag{18}$$

where T_0 represents the fundamental period, V_n denotes the n-th interharmonic voltage amplitude, and V_1 signifies the fundamental voltage amplitude.

The above derivation demonstrates that the PSD variance of the system frequency deviation is influenced by several factors: wind power fluctuation, synchronous generator characteristics, energy storage transfer function, system inertia constant, and load frequency coefficient. Notably, a larger PSD $S_w(f)$ of wind power fluctuation corresponds to a larger variance in the PSD of system frequency deviation, indicating increased instability in system frequency. The variance of the system frequency deviation PSD is inversely proportional to the energy storage transfer function. Furthermore, when deriving the other three power quality indices, the relationship between spectrum and power spectrum is utilized. This analysis reveals that the three-phase THDi and $\cos\varphi$ of the system generator are consistent with $PSD(I_1)$, where $PSD(I_n)$ is directly related. THDi is directly proportional to $PSD(I_n)$, while $\cos\varphi$ defines the relationship between harmonics and the power factor. In the rectification stage, it is deduced that it is inversely proportional to $PSD(I_n)$. Additionally, an increase in harmonic current leads to an increase in distortion power D, which consequently decreases the power factor. Based on the theory that interharmonics affect voltage fluctuation, it is shown that different interharmonic voltage amplitudes influence the magnitude of voltage fluctuation, with a larger $PSD(V_n)$ resulting in a larger d_{RMS}.

This study demonstrates a correlation between PSD and power quality indices through the development of mathematical derivations for the system. The research also reveals that these factors are influenced by energy storage systems, power electronic devices, wind power fluctuations, and load disturbances.

2.3 Power Spectrum Simulation and Wind Power System Analysis

The wind power hybrid energy storage system model was constructed using the Simulink platform, incorporating components such as wind turbines, energy storage devices (batteries and supercapacitors), power electronic devices (rectifiers), load models, and power electronic control systems. The model development considered several factors, including the system's dynamic characteristics, control strategies, and component interactions. It simulated wind speed fluctuations, load variations, and charge-discharge processes of the energy storage system. Additionally, the model recorded system spectra and power quality indices, such as the harmonic content and voltage fluctuations. During the simulation, spectrum analysis software calculated the power spectrum of the output power signal, determining the system's energy distribution across different frequencies and revealing its frequency-domain characteristics. Through analysis of the simulation results, the study established the correlations between power spectrum characteristics and power quality indices of wind power hybrid energy storage systems.

As illustrated in Fig. 1, the single-phase current spectrum diagram of the permanent magnet synchronous generator under random wind conditions reveals that the generator's THDi is 18.57%. This distortion primarily consists of the 5th, 7th, 11th, and 13th harmonics, which correspond to the typical characteristics of nonlinear loads and switchgears in power systems. The harmonic content decreases progressively with increasing frequency. In terms of spectral energy distribution, the low-frequency range (near 50 Hz) exhibits the highest amplitude ratio, attributable to the fan's output being predominantly concentrated at the fundamental frequency. In the mid-frequency range (100–400 Hz), several significant harmonic peaks are observed, indicating the influences of wind speed fluctuations and nonlinear control devices on the system. The high-frequency range (above 400 Hz) contains less harmonic content, although some small-value components persist, possibly resulting from rapid switching actions or other high-frequency interferences. The high harmonic content may impact the system's power quality, potentially causing issues such as equipment heating and power factor reduction.

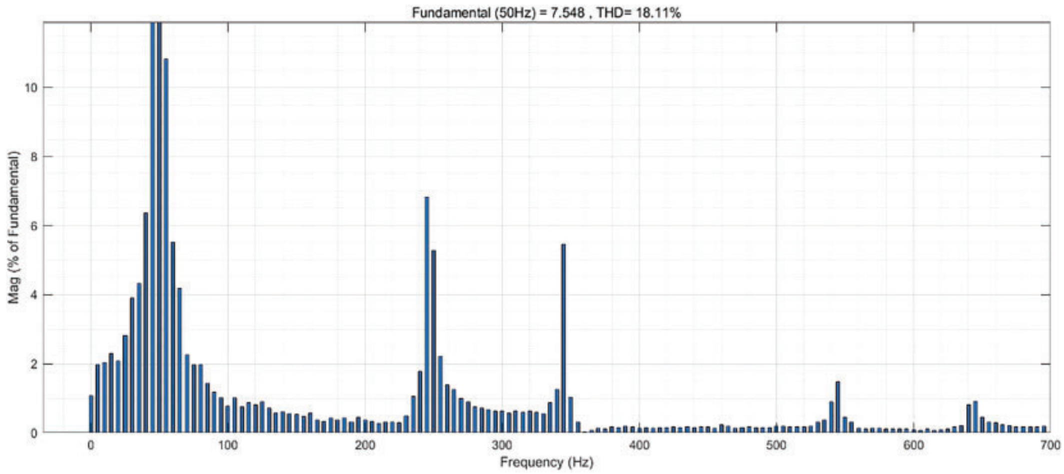

Figure 1: Single-phase current energy distribution with frequency

Likewise, Fig. 2 indicates the impact of energy storage on voltage fluctuation and frequency stability when wind speed varies. The results demonstrate that wind speed fluctuates at 2 and 4 s, with wind power decreasing from 450 to 380 W, indicating significant volatility. The total harmonic distortion rate of the generator's three-phase current ranges from 24.81% during the 2–4 s period to 13.45% after stabilizing at 4 s, primarily due to reduced subharmonic and interharmonic wave content. Concurrently, the load voltage fluctuates, decreasing from 55 to 54 V, with increased amplitude compared to the 2–4 s period. This causes the lithium battery power to drop from −300 to −200 W to maintain system balance. In comparison, the supercapacitor's power decline is minimal, only 5 W, but its energy storage effect in maintaining system energy balance is rapid. Notably, it supplements load power loss in less than 0.1 s, preventing load voltage fluctuations and system instability, thereby enhancing the system's power quality.

Furthermore, an unsteady source-storage-load experimental platform revealed variations in the output power quality indices when the wind power system lacked energy storage. Upon incorporating different energy storage devices and utilizing the AR model to estimate the PSD of the data, the frequency-domain transformation trend of the power quality indices in the wind power system decreases. Moreover, this approach provides a more comprehensive understanding of the power quality indices and power spectrum characteristics of wind power hybrid energy storage systems, offering an effective and reliable method for evaluating and enhancing the output power quality of wind power systems.

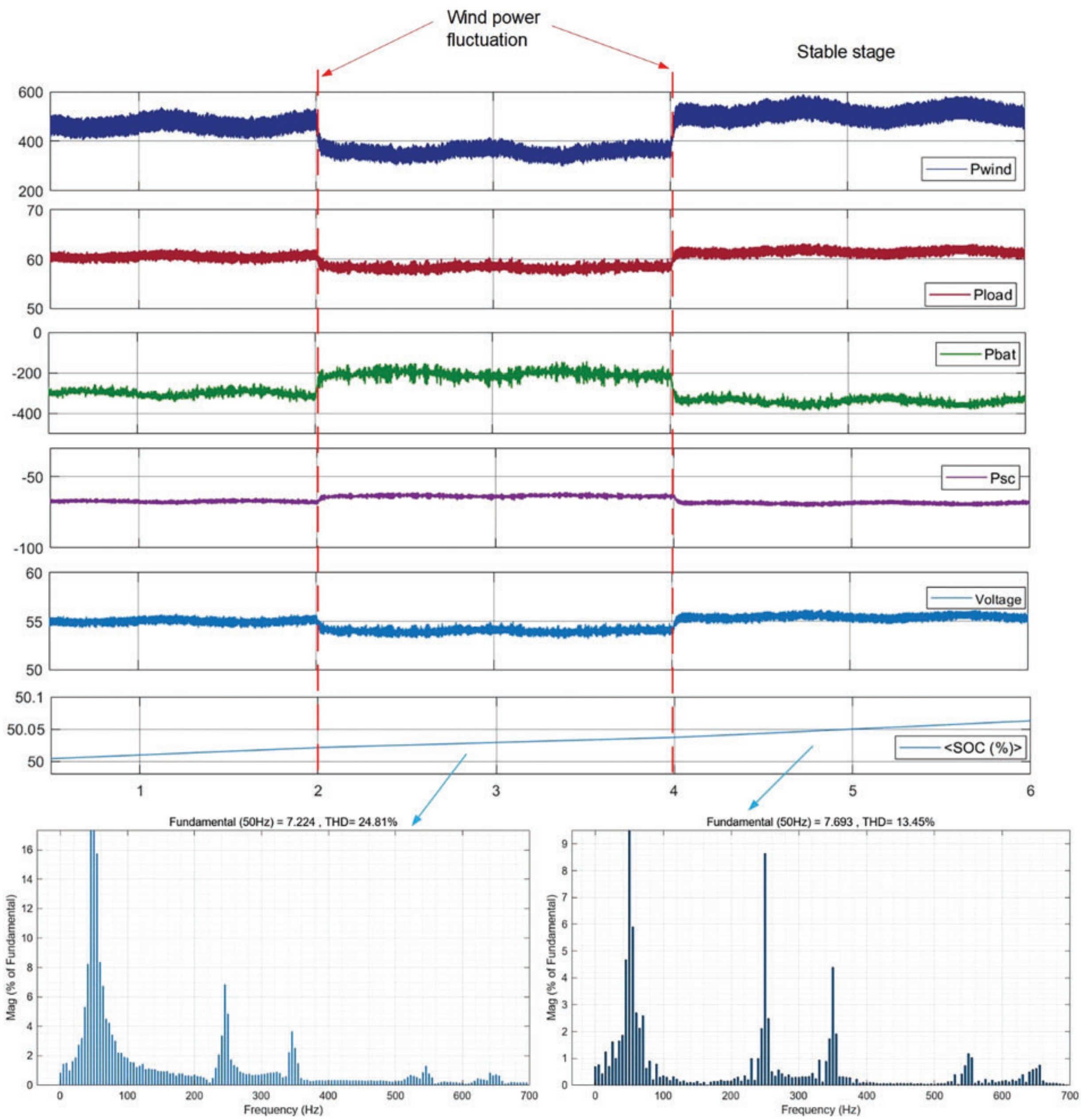

Figure 2: Diagram of the influence of charge and discharge on voltage fluctuation and frequency stability

3 System Power Quality and Power Spectrum Analysis Experiment

This study's experimental setup was arranged as shown in Fig. 3. The research focused on observing the harmonic mode, frequency changes, and harmonic numbers of the power signal. Additionally, the PSD of the AR model was estimated to verify the relationships between the power quality indices and PSD. The experiment utilized a wind tunnel platform to provide relatively stable incoming air. A wind wheel was connected to the generator through a torque meter, with the output connected to a rectifier and then to a DC load box for no-energy storage experiments. Energy storage experiments were conducted by connecting various devices (including lithium batteries, supercapacitors, and heat storage devices). The generator output voltage, current, and other parameters were recorded using a DH5902 data acquisition and analysis system, a Fluke Norma 5000 power analyzer, and other experimental instruments. The equipment was set to harmonic mode to monitor frequency changes and harmonic frequencies of the power signal. The DC load box and Fluke data recording were adjusted for unsteady state experiments. Tests were conducted within a wind speed range of 8 to 12 m/s, with the generator speed adjusted from 100 to 600 rad/min through the DC load box to examine performance under varying wind speeds.

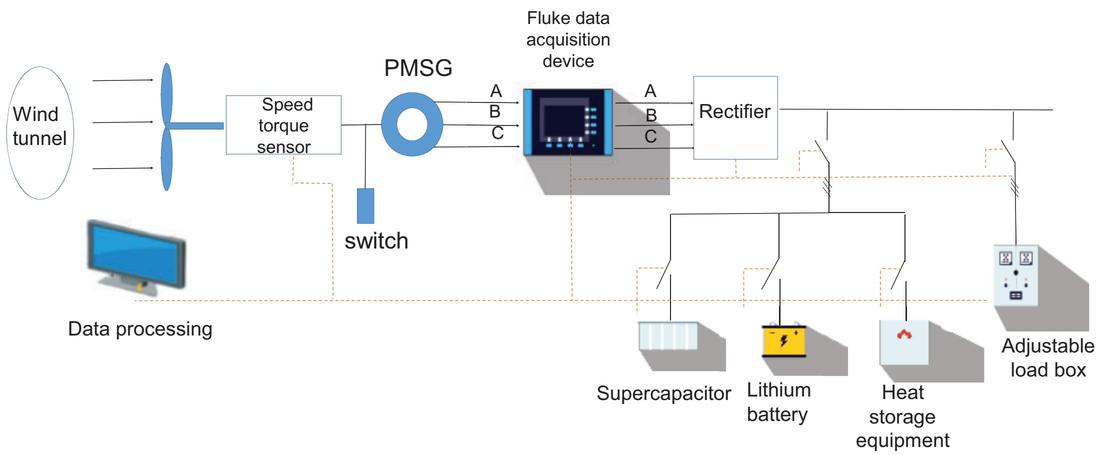

Figure 3: Experimental test system diagram

3.1 No-Energy Storage Power Quality Index Characteristics Experiment

This study investigated the correlation between power quality and load at varying wind speeds. The experiment was conducted at and above the rated wind speed to explore the relationships among power quality evaluation indices, loads, and wind speeds under different conditions. Four representative power quality evaluation indices were analyzed: THDi, frequency deviation ratio, voltage fluctuation, and power factor $\cos\varphi$. THDi was calculated using the average of 10 non-overlapping measurement periods, as per Reference [28]. d_{RMS} represents the effective value of the mean-root curve of voltage square, observed over 10 consecutive measurement periods, which was calculated according to the Voltage Fluctuation and Flicker of Power Quality method described by Reference [29]. Similarly, the average value of $\cos\varphi$ was determined from 19 random time points, following the Method for Measurement and Evaluation of Power Quality of Wind Turbines. The frequency deviation ratio was derived by comparing the frequency deviation with the system's nominal frequency. The relationship between speed n and pole logarithm p indicates that the generator's voltage fundamental frequency at different speeds aligns with the system's normal frequency, as shown in Fig. 4.

Analysis of Fig. 4a reveals that THDi initially decreases and then increases, reaching its lowest value at 150 W under a 10 m/s load. At constant loading, THDi slightly increases when wind speed is at its minimum. THDi is notably influenced by load, with a more pronounced upward trend observed beyond 200 W. Fig. 4b demonstrates that under consistent load conditions, voltage fluctuation exhibits a positive correlation with wind speed, increasing by 0.2%–0.3%. Voltage fluctuation is also affected by load, reaching its minimum between 150 and 200 W at a constant wind speed. Fig. 4c primarily illustrates the impact of load. Under steady wind speed, the trend initially increases before stabilizing. The maximum value of 94% is achieved when the load reaches 200 W. Conversely, at constant load, $\cos\varphi$ displays an upward trend with increasing wind speed, albeit with minimal change, approximately 1% overall. Fig. 4d indicates that the frequency deviation ratio's variation trend mirrors that of voltage fluctuation. The key distinction is that under consistent load conditions, the amplitude of voltage fluctuation exceeds the frequency deviation ratio as wind speed increases. In the absence of energy storage, the power quality indices are primarily influenced by changes in wind speed and generator speed. As generator speed is adjusted by modifying the load during the experiment, harmonic content, voltage fluctuation, and frequency deviation increase with speed under constant wind conditions before the rated speed is reached.

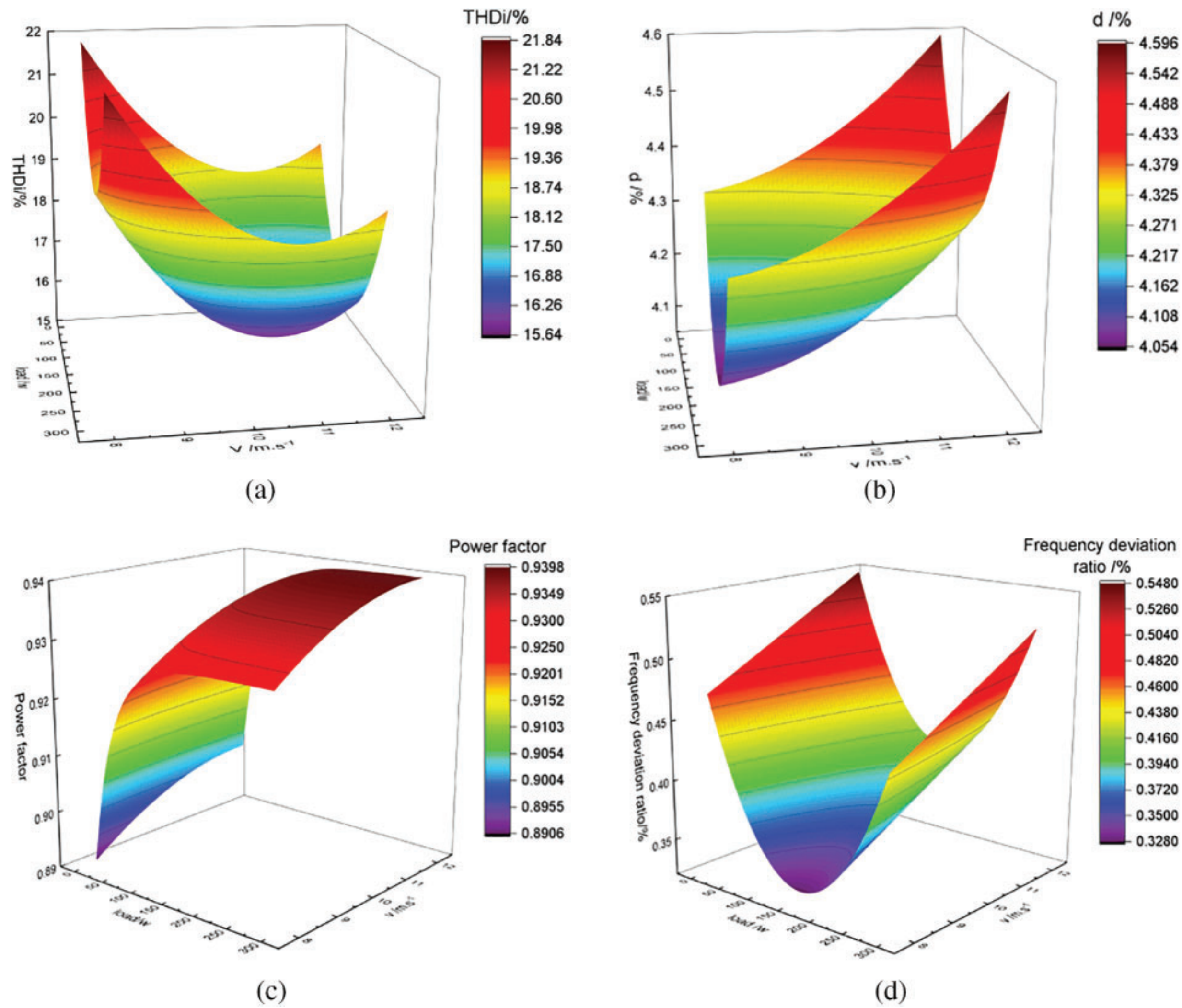

Figure 4: Experimental test diagram of power quality indices without energy storage. (a) THDi; (b) voltage fluctuation; (c) power factor; (d) frequency deviation ratio

However, the corresponding fundamental frequency and nominal voltage value increased more rapidly, resulting in a reduced THDi, d%, and frequency deviation ratio. Upon reaching the rated speed, the output rated power is stabilized, contributing to reduced voltage fluctuations, total harmonic distortion rate, and frequency deviation of the current. The power quality analyses illustrated in Fig. 4a,b,d all reach their lowest points. After exceeding the rated speed, alterations in the electromagnetic field distribution within the generator lead to increased harmonic generation. In variable-speed wind turbines, speed changes affect the response of the control system, potentially increasing the distortion of current and voltage waveforms, thus elevating harmonic content. Nevertheless, it is observed that the growth of fundamental frequency and nominal voltage decelerates. $\cos\varphi$ ceases to increase while the other power quality indices in the graphs exhibit increases. This observation aligns with the previously derived relationship, further validating its accuracy.

Conversely, under constant load conditions, an increase in wind speed leads to a decline in power quality, particularly when the wind speed reaches 11–12 m/s. This phenomenon is attributable to several factors. The significant fluctuations in wind speed, combined with the nonlinearity of power electronic devices in the rectifier, result in distortion of the three-phase waveform and generation of harmonics. Consequently, the generator's output power becomes unstable. The presence of harmonics may increase the system's reactive power demand and reduce the fundamental wave factor, potentially impeding further improvement of the power factor. Furthermore, without an energy storage system to balance the energy, the load voltage and power are susceptible to instability and fluctuations. These factors collectively contribute to a decrease in the overall system's power quality.

3.2 Power Quality Index Characteristics Experiment under Different Energy Storage Forms

This paper examined the impact of various energy storage systems, including lithium batteries, heat storage, supercapacitors, and a hybrid of lithium batteries and supercapacitors, on improving power quality. Fig. 5 illustrates that THDi decreases as the blade tip speed ratio (λ) increases under unsteady state conditions. The addition of energy storage devices to the system demonstrates that hybrid energy storage significantly outperforms other storage types in reducing THDi within the λ range of 3.0–5.0, with supercapacitors slightly surpassing lithium batteries. At higher blade tip speed ratios, the effectiveness of all three energy storage systems diminishes. In the λ range of 3.0–4.0, when the generator achieves the rated speed, conversion efficiency peaks, potentially resulting in more stable power output and the most rapid decrease in system THDi. In this range, generator speed remains relatively constant, with λ primarily influenced by the wind speed. Supercapacitors can respond swiftly to reduce THDi and enhance power quality. However, variations between intervals are mainly affected by the motor speed. During this process, lithium batteries can absorb excess energy generated and maintain system stability. As λ continues to increase beyond the rated value, the system generator becomes overloaded, compounded by wind speed and velocity influences, causing THDi to rise. At this point, energy storage responds rapidly to suppress system harmonics, though this impacts the lifespan of the energy storage equipment. The frequent occurrence of harmonics necessitates continuous short-term, high-frequency charging and discharging of the energy storage system, particularly for supercapacitors, which typically handle a higher proportion of harmonic suppression tasks due to their rapid charge and discharge capabilities. This high-frequency operation mode increases heat accumulation in the energy storage device, accelerating internal material aging, such as electrolyte deterioration and plate loss. These phenomena directly lead to decreased energy storage equipment capacity, increased internal resistance, and shortened service life. Regarding long-term system maintenance and efficiency impacts, the reduced lifespan of energy storage systems necessitates more frequent replacement of batteries or other energy storage components, increasing maintenance costs. Furthermore, the degradation of energy storage equipment performance may result in diminished harmonic suppression effectiveness, leading to decreased system power quality and compromised stability and reliability.

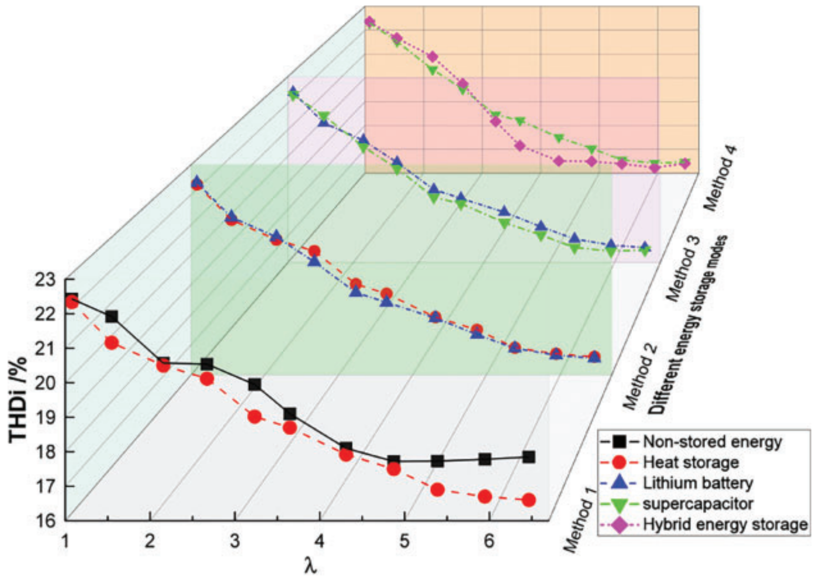

Figure 5: Comparison of THDi values of different energy storage forms

Similarly, Fig. 6 demonstrates a negative correlation trend between d and λ. Following the addition of the energy storage device, the system voltage fluctuation decreases from a λ range of 3.6–7.0. Increased energy storage can reduce d by approximately 0.5%. Lithium batteries and supercapacitors exhibit comparable effects in improving d, while hybrid energy systems demonstrate superior performance in reducing d compared to other single-energy storage methods. When λ ranges from 6.0–7.0, a gradual decreasing trend in d is found. When λ is low, the wind turbine blades rotate slowly relative to wind speed, resulting in inefficient conversion of wind energy into rotational energy. This leads to reduced aerodynamic efficiency of the blades, unstable power output, and the inability of battery energy storage to promptly accommodate system power changes, resulting in a large d. Supercapacitors more effectively suppress short-term voltage fluctuations due to their rapid response capabilities, although fluctuations may persist over longer timescales. When λ is excessively high, the blade speed becomes too fast, subjecting the blade tip to significant aerodynamic resistance and eddy current loss. Consequently, a portion of the wind energy cannot be effectively converted into mechanical energy. In this scenario, the fan's aerodynamic efficiency is poor, and power output fluctuations are more severe. Supercapacitors can respond to power fluctuations rapidly and reduce d, but d may remain substantial due to the inherent volatility of wind speed and power changes. Battery energy storage may face slow response issues, potentially resulting in more pronounced voltage fluctuations. Hybrid energy storage combines the long-term energy regulation capabilities of lithium batteries with the advantages of supercapacitors in rapidly responding to short-term power fluctuations, achieving effective suppression of d.

Fig. 7 illustrates that $\cos\varphi$ exhibits the most rapid growth rate when λ is in the 3.0–4.0 range. The growth rate tends to decelerate around 5.0. Although hybrid energy storage can continue to enhance the system's power factor, with the maximum value exceeding 0.90, in this range, lithium batteries demonstrate a marginally superior improvement effect compared to supercapacitors. The current speed and $\cos\varphi$ are correlated. The frequency and current generated by the permanent magnet synchronous generator are directly influenced by its rotational speed. If the rotational speed is below the rated speed, the power factor will be affected due to distortion in the output current and frequency fluctuations. The primary function of energy storage is to improve power quality and mitigate system volatility.

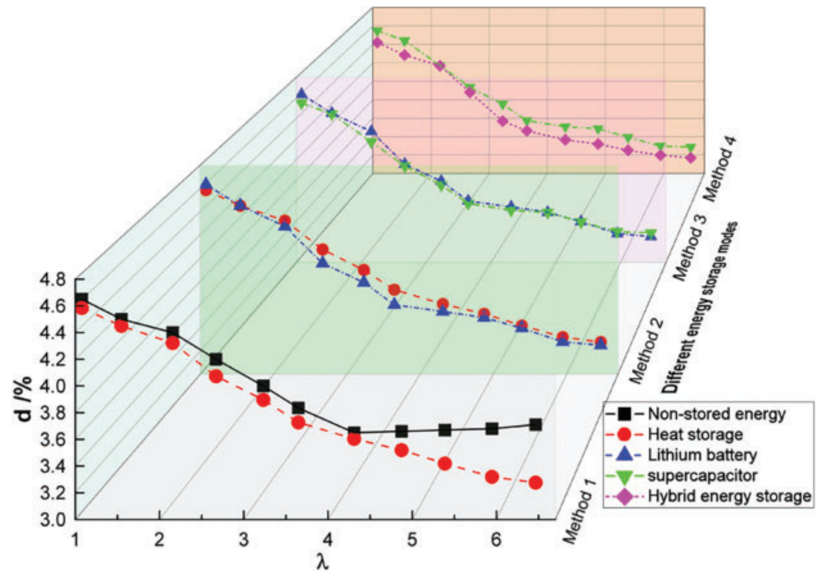

Figure 6: Comparison diagram of voltage fluctuations of different energy storage forms

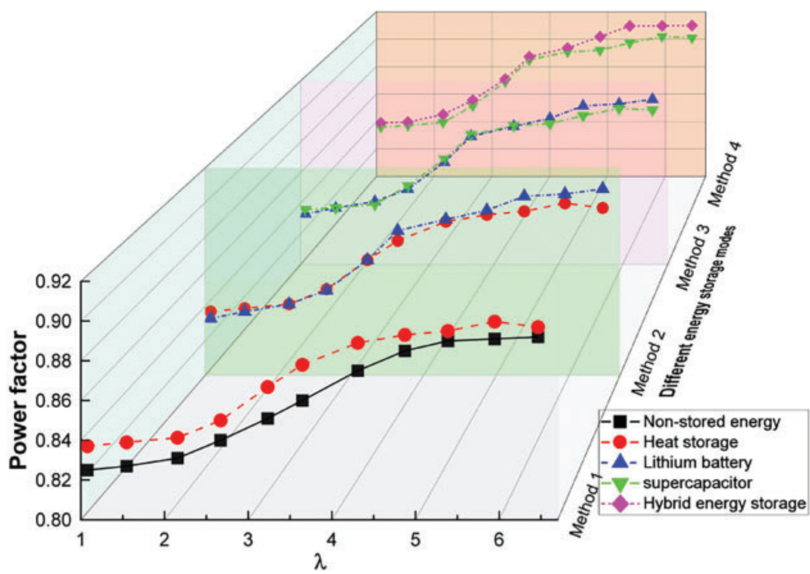

Figure 7: Comparison diagram of power factors of different energy storage forms

Fig. 8 demonstrates that, without energy storage, the frequency deviation ratio progressively decreases as λ rises, then slightly increases after λ reaches 3.7. Upon the addition of an energy storage device, the frequency deviation ratio drops to 0.25. Hybrid energy storage exhibits a superior improvement effect compared to single energy storage options, with supercapacitors showing a marginally better effect on reducing frequency deviation than heat storage and lithium batteries. Heat storage and lithium batteries demonstrate comparable effects in lowering the frequency deviation ratio. This experiment, conducted in a wind tunnel, provides a more realistic simulation of wind speed fluctuations and volatility. As λ increases significantly, the system experiences high-frequency power fluctuations. Supercapacitors can provide rapid and sufficient power in short periods, thereby suppressing frequency fluctuations caused by wind speed variations. The hybrid energy storage system can more effectively manage power fluctuations and frequency deviations across different time scales. Consequently, supercapacitors are particularly effective in handling frequency deviations, especially those involving high-frequency, rapid power fluctuations, while lithium batteries and thermal energy storage address energy management over longer time scales.

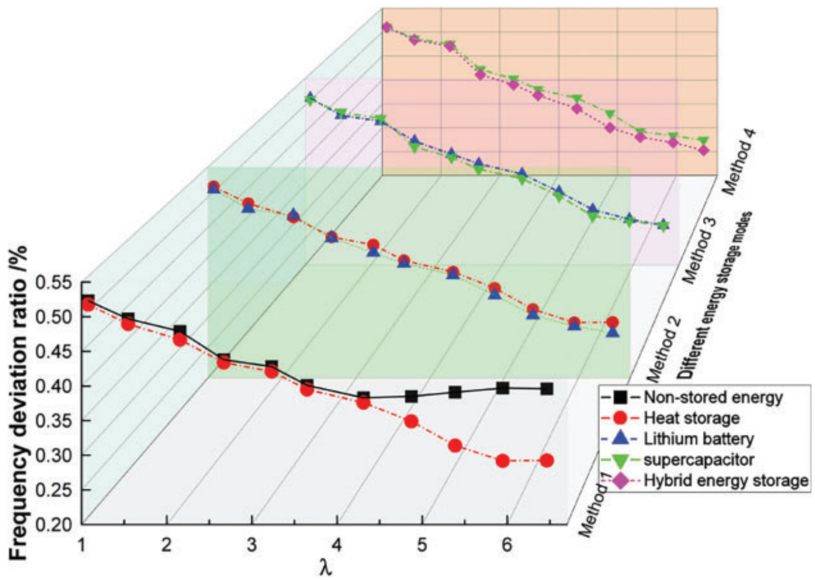

Figure 8: Comparison diagram of frequency deviation ratios of different energy storage forms

In conclusion, the hybrid energy storage system, which combines different energy storage devices such as batteries and supercapacitors, offers distinct advantages over single energy storage solutions. This system enhances the ability to manage load fluctuations and wind power instability, thereby mitigating economic losses associated with power supply interruptions. Moreover, it circumvents the need for higher capacity redundancy often required by single energy storage devices, thus reducing initial investment costs. From a frequency-domain perspective, the hybrid energy storage system minimizes battery cycle depth by allocating high-frequency power fluctuations to rapid-response supercapacitors, while low-frequency fluctuations are managed by the battery. This strategic distribution extends battery service life and reduces long-term operational expenses.

3.3 Correlation Analysis of Power Quality and Power Spectrum Characteristics

This research analyzed the fluctuations of wind power output and their effects on system stability, investigating how energy storage systems could effectively mitigate power fluctuations while enhancing the system's power quality. The hybrid energy storage system was influenced by the power quality indices, energy storage capacity, and system volatility. The study examined the current signal of the generator at the rated speed and its power spectrum. The figure below shows a comparison between different energy storage modes and the single-phase current spectrum without energy storage. After the generator reaches the rated speed, the fundamental frequency is 50 Hz. Due to wind speed fluctuations, the generator-side power signal produces 5th, 7th, 11th, and 13th harmonics, as well as some interharmonics, under no-storage conditions. Upon introduction of the energy storage system, the harmonic energy decreases due to the energy's fundamental frequency. Fig. 9 demonstrates that the lithium battery primarily suppresses harmonics in the 0–255 Hz frequency range. Notably, the fifth harmonic is suppressed, with its amplitude decreasing from 0.77 to 0.5, resulting in a harmonic reduction ratio of 60%. In Fig. 10, the suppression range of heat storage is mainly concentrated in the 250–500 Hz range. Similarly, Fig. 11 reveals that after adding the supercapacitor, the highest frequency harmonics are suppressed, the 11th harmonic frequency is reduced, and the 13th harmonic experiences the largest decline, with its amplitude approaching zero. The frequency spectrum characteristics of the generator's output current signal align with the simulation results of the wind turbine's three-phase current in the previous simulation system, confirming that energy storage can reduce the signal's harmonic energy and increase the proportion of fundamental wave energy.

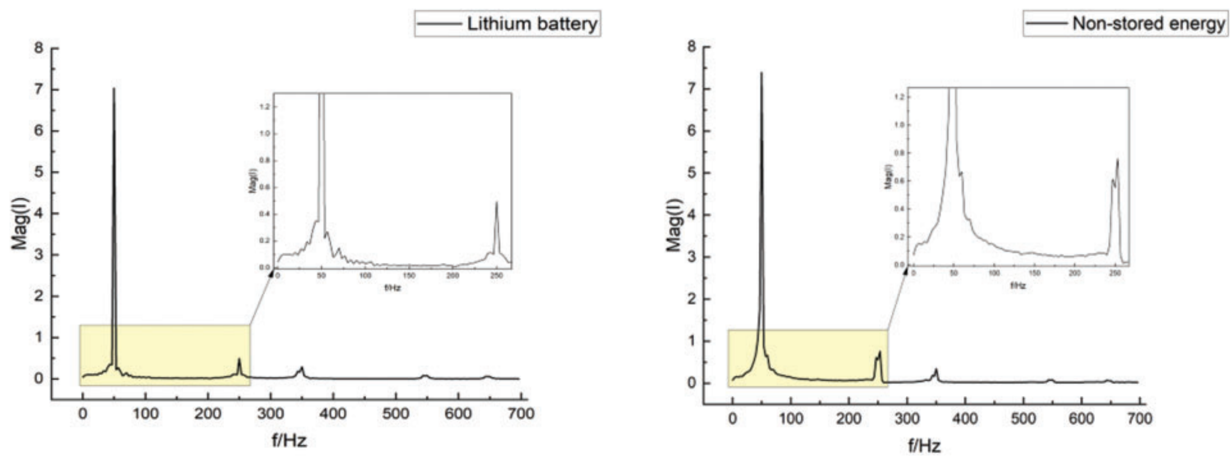

Figure 9: Spectrum comparison between lithium battery and no-energy storage

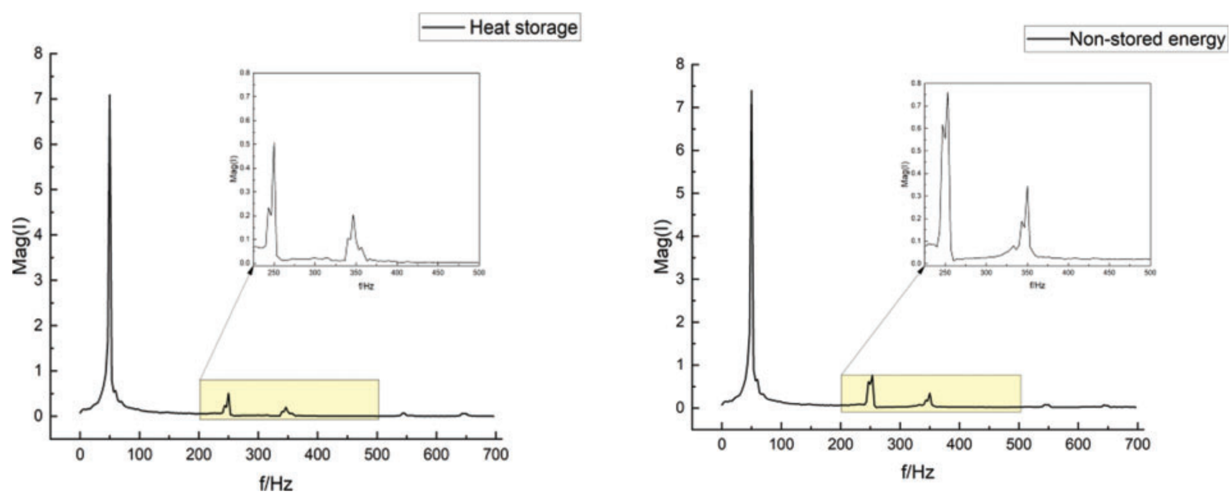

Figure 10: Spectrum comparison between heat storage and no-energy storage

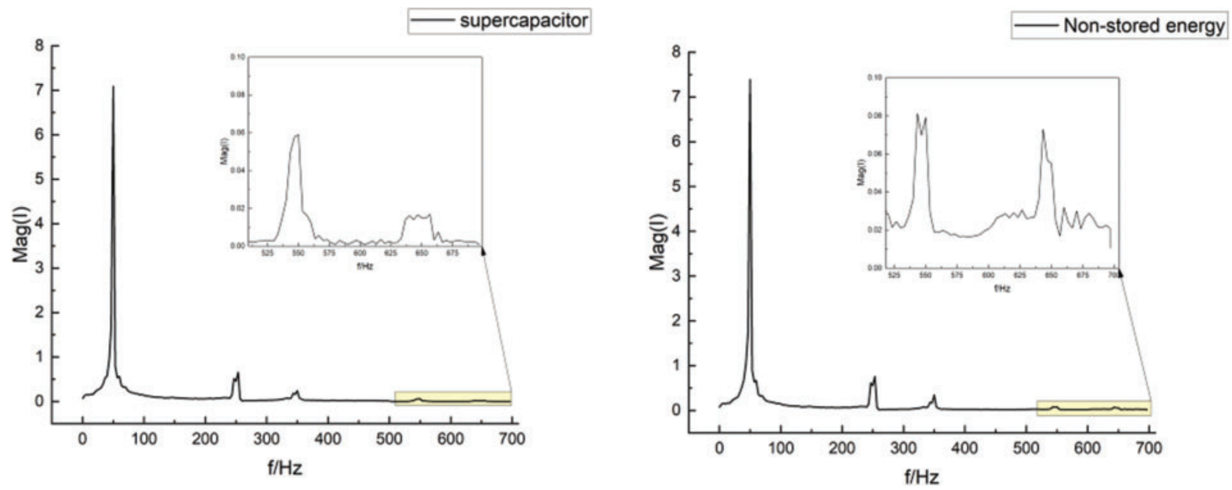

Figure 11: Spectrum comparison between supercapacitor and no-energy storage

Moreover, Fig. 12 presents the variance comparison of PSD with various energy storage frequencies. Without energy storage, the system frequency deviation exceeds the fluctuation, with the frequency deviation ratio surpassing ±0.005 at certain points. The addition of energy storage devices notably mitigates frequency deviation ratio fluctuations. Lithium batteries demonstrate the most significant reduction in frequency deviation ratio, while heat storage and supercapacitors exhibit relatively higher ratios at specific moments. The variance of the system frequency deviation PSD decreases from 0.000790228 without energy storage to 0.000520593 for heat storage, 0.000507921 for lithium batteries, and 0.000585 for supercapacitors. The introduction of energy storage devices gradually stabilizes the system frequency. Key observations include:

(1) Following the conversion using Eq. (1), the current signal and THDi of the generator increase, primarily due to the influence of harmonics and frequency. The increase in each harmonic content leads to an increase in overall distortion. This phenomenon is attributed to the converter's on-off operation, which produces a non-sinusoidal waveform, resulting in a three-phase electric current containing multiple frequency components of the complex waveform, including harmonic components. This process of harmonic generation was previously discussed by Reference [30]. Notably, the harmonic amplitude decreases as the harmonic order increases [31]. Concurrently, wind speed variability causes fluctuations in wind power, which subsequently affects the wind turbine's output power. These rapid fluctuations in power output contribute to the distortion of the system's harmonic current and voltage waveforms.

(2) The impact of voltage fluctuation primarily manifests in wind speed variations, which subsequently affect wind turbine power output. After rectification, the bus voltage also changes, increasing inter-harmonic content corresponding to the rise of $PSD(V_n)$, resulting in varying degrees of voltage fluctuations. In the hybrid energy storage system, wind speed randomness influences the system's energy balance. Through precise control of the energy storage system, internal energy can be rapidly transformed to meet the system's energy balance requirements, maintain stable voltage at the load end, and enhance power quality [32]. These findings align with the simulation results of voltage fluctuation caused by energy storage charge and discharge cycles.

(3) The energy storage device rapidly responds to wind power system demands, balancing fluctuations by absorbing or releasing energy, thereby reducing system frequency deviations. As illustrated by the power spectrum analysis in Figs. 9–12, the incorporation of energy storage redistributes energy across frequency bands, enhancing fundamental frequency energy while decreasing the variance of

the system frequency deviation PSD. This results in improved system frequency stability and power quality. Consequently, effective configuration and control strategies for the energy storage system are critical for maintaining power grid frequency stability.

(4) The generation of harmonics in the system leads to distortion power D, resulting in a significant phase offset between the terminal voltage and current. This offset causes the power factor to decrease below the neutral value of 0.9. The power factor is a crucial characteristic of power users, as a lower value can unnecessarily burden synchronous generators and electric transmission lines [33]. In wind power hybrid energy storage systems, odd harmonics are frequently generated due to wind power fluctuation and converter influences. A higher harmonic content leads to a lower $PSD\,(I_1)$, increased distortion power D, and a larger phase offset. However, the energy storage system demonstrates a notable capacity to suppress harmonics, thereby enhancing the power factor and improving overall power quality.

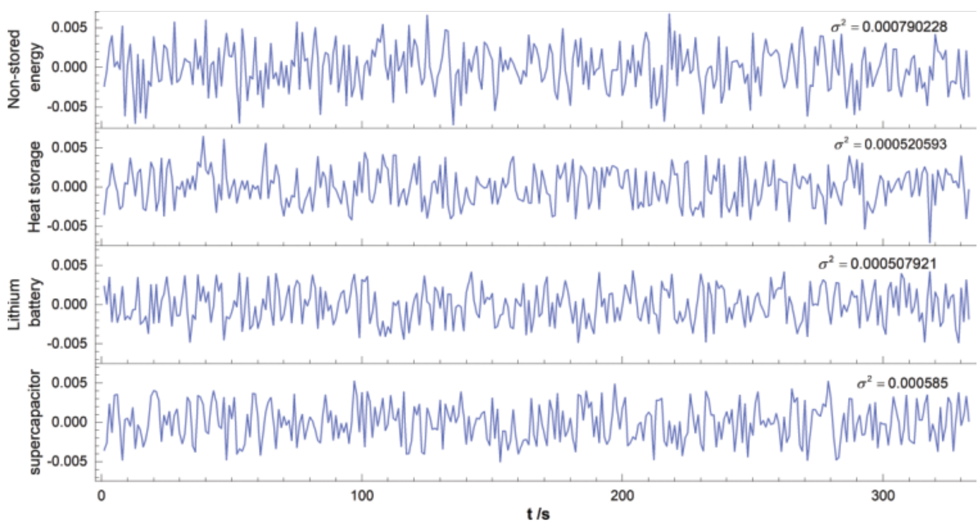

Figure 12: Variance comparison of PSD with different energy storage frequency deviations

4 Multi-Objective Optimization

This section elucidated the relationships between the system signal value and the power quality indices by modifying the order of the AR model in power spectrum estimation parameters. Through Matlab algorithm programming, this relationship was applied to NSGA-II, MOEA/D, and GA + Pareto optimization algorithms to optimize the power quality indices. This process enabled the system to explore multiple solution combinations, aiming to achieve optimal performance across various power quality metrics. The specific optimization process is illustrated in Fig. 13.

The optimization algorithm incorporated four power quality indices: frequency deviation, THDi, cos φ, and d%. These indices served as objective functions f_1, f_2, f_3, and f_4, respectively. The objective function relationships were derived from Eqs. (9), (11), (13) and (18), based on which the following multi-objective function was formulated:

$$\begin{aligned} f &= f\left(f_1, f_2, f_3, f_4\right) \\ &= \min\left[f_1 + f_2 - f_3 + f_4\right] \end{aligned} \tag{19}$$

The specific decision variables encompassed the AR model order, wind speed, and wind power.

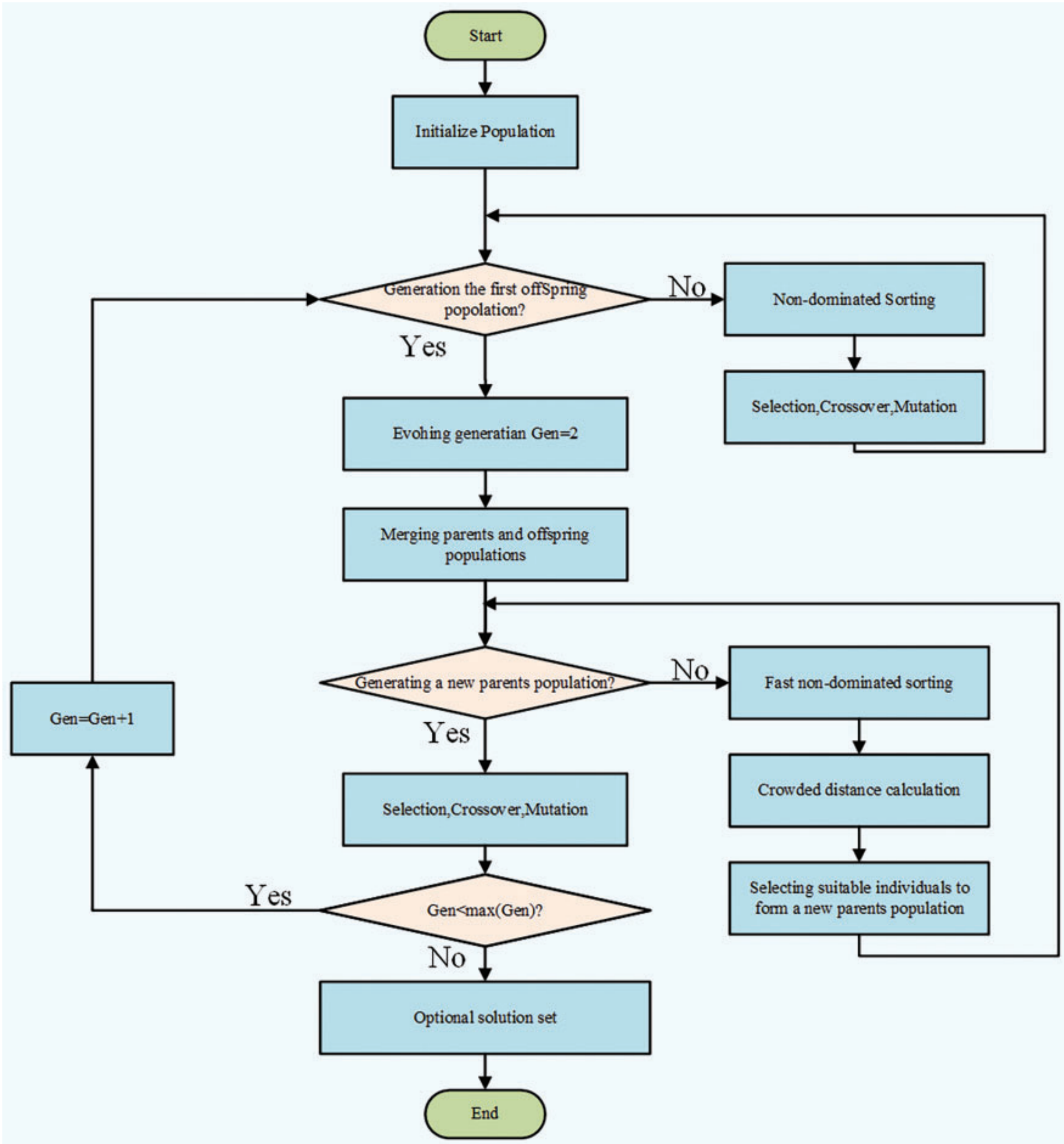

Figure 13: NSGA-II multi-objective optimization flow chart

Simultaneously, several constraints were implemented to ensure the accuracy and stability of power spectrum estimation. The order n of the AR model was subject to the following constraint:

$$45 \leq n \leq 75 \tag{20}$$

THDi was calculated using the following equation:

$$0 \leq THDi \leq 12\% \tag{21}$$

The voltage fluctuation was determined based on

$$|d| \leq 7\% \tag{22}$$

The wind speed range was calculated using Eq. (23) to ensure the feasibility, practicability, and safety of the power quality optimization results.

$$7m/s \leq v \leq 9m/s \tag{23}$$

The algorithm iterated 500 times, with the distance between individuals reflecting the algorithm's diversity and convergence. A higher number of individuals with large distances indicates greater diversity, while a higher number of individuals with small distances and high aggregation suggests stronger correlation and improved convergence. Tables 1 and 2 illustrate the diversity and convergence of the three algorithms for orders 45 and 75, respectively. Following multi-objective optimization, the distribution of optimal solutions for different objective functions was depicted in three-dimensional space, as shown in Fig. 14.

Table 1: Diversity and convergence for an AR model order of 45

Distance	NSGA-II	MOEA/D	GA + Pareto
0–0.2	445	455	454
0.2–0.4	35	37	33
0.4–0.6	10	4	10
0.6–0.8	7	4	3
0.8–1.0	1	1	0
1.0–1.2	2	0	0

Table 2: Diversity and convergence for an AR model order of 75

Distance	NSGA-II	MOEA/D	GA + Pareto
0–0.2	427	440	435
0.2–0.4	37	40	39
0.4–0.6	19	8	16
0.6–0.8	12	9	8
0.8–1.0	3	1	1
1.0–1.2	2	2	1

(1) Diversity analysis results

As the order of the AR model increases from 45 to 75, the number of high-distance individuals utilized to measure the relative differences in the target space significantly increases. This observation indicates that the algorithm can explore more diverse solutions, thereby enhancing the likelihood of identifying the global optimal solution. Irrespective of the AR model order, NSGA-II consistently demonstrates a higher number of individuals in the high-distance interval (0.6–1.2) compared to MOEA/D and GA + Pareto. This suggests that NSGA-II maintains superior diversity in its solution set.

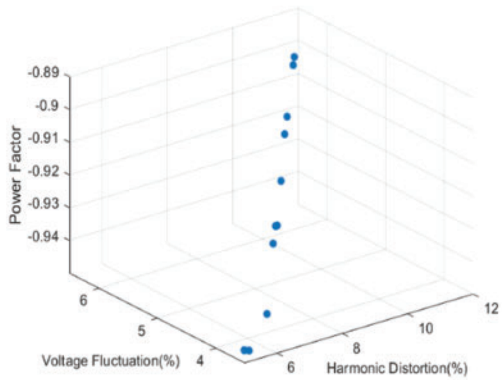

(a1)

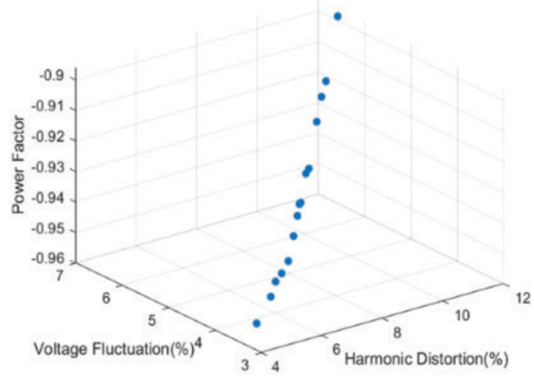

(b1)

NSGA-II

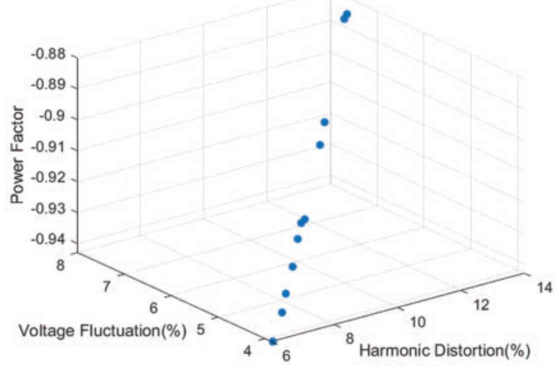

(a2)

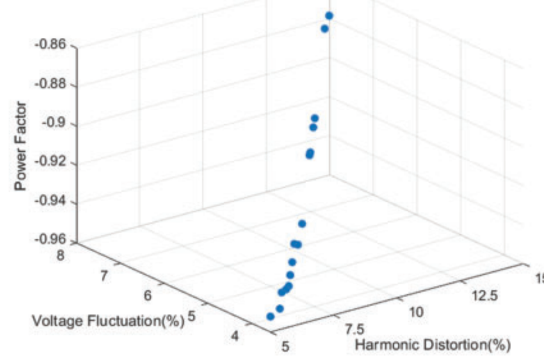

(b2)

MOEA/D

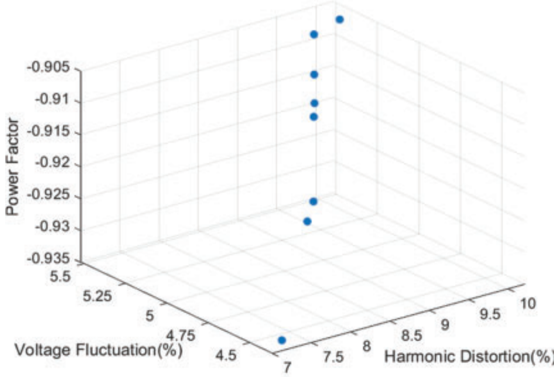

(a3)

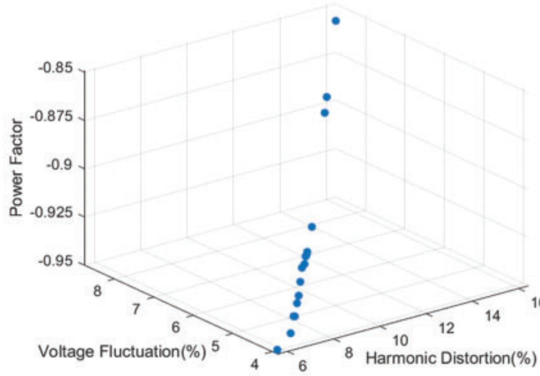

(b3)

GA+Pareto

Figure 14: Distribution of optimal solutions of the three algorithms

(2) Convergence analysis results

At an order of 45, NSGA-II exhibits marginally fewer individuals in the 0–0.2 distance range compared to MOEA/D while showing similar performance to GA + Pareto. When the order increases to 75, MOEA/D performs superior to NSGA-II in the low-distance range. Overall, the MOEA/D algorithm displays higher convergence.

(3) Optimal solution analysis results

Fig. 14 shows the distribution of optimal solutions for different objective functions in a three-dimensional space. In Fig. 14a, the AR model has an order of 45, while in Fig. 14b, the AR model has an order of 75. The results indicate that when the order of the AR model increases from 45 to 75, the number of optimal solutions for each power quality index increases by 36%, and the clustering degree of different solutions is also higher. Compared to the other two algorithms, NSGA-II demonstrates greater diversity, with a more uniform distribution of different solutions. The number of NSGA-II's solutions with $\cos \varphi$ exceeding 0.9 is significantly higher than that of the other two algorithms, achieving optimal power quality indices of THDi (4.62%), d% (3.51%), and $\cos \varphi$ (96%). MOEA/D exhibits higher convergence, with a more aggregated distribution of different solutions, and demonstrates optimal power quality indices of 5.03%, 3.58%, and 95%, although including solutions with $\cos \varphi$ below 0.9. The GA + Pareto algorithm yields inferior optimal solutions compared to the other two algorithms.

5 Conclusion

This study employed the correlation theory of spectra, PSD, and random signal power spectra to derive the relationships between the system's output power quality indices and PSD. These relationships were subsequently validated through experimental and simulation methods. Ultimately, the established relationships were utilized for multi-objective optimization, where various optimization algorithms were compared to achieve optimal system power quality. The specific conclusions are as follows:

(1) Correlation between power quality and power spectrum

Wind power variability contributes to power quality fluctuations by influencing the PSD. This impact manifests as increased frequency deviation, heightened voltage fluctuation, elevated THDi, and reduced power factor ($\cos \varphi$). The integration of energy storage equipment significantly mitigates system frequency fluctuations and harmonic components while improving the power factor. These results underscore the critical role of energy storage in optimizing power quality.

(2) Optimization effect of energy storage system on power quality

Lithium batteries and supercapacitors substantially enhance system stability by swiftly responding to power fluctuations induced by wind speed variations, effectively mitigating THDi and d%. The hybrid energy storage system integrates the long-term energy regulation capacity of lithium batteries with the rapid response capability of supercapacitors. This combination achieves notable improvements in power quality across multiple time scales, particularly in diminishing harmonic distortion rates and voltage fluctuations.

(3) Comparison of multi-objective optimization algorithms

As the order of the AR model increases, the diversity and convergence of the three algorithms significantly improve. From the perspective of optimal solution distribution, NSGA-II demonstrates the best diversity performance, while MOEA/D exhibits superior convergence. However, practical applications reveal that despite its enhanced convergence, MOEA/D is less effective than the NSGA-II algorithm in obtaining the optimal solution. The optimum power quality indices achieved by NSGA-II are as follows: THDi of 4.62%, d% of 3.51%, and $\cos \varphi$ of 96%.

This study uniquely combines PSD theory with power quality optimization, proposing a multi-objective optimization framework. This approach not only addresses the impact of wind power fluctuation on power quality but also offers a novel perspective for optimal energy storage system configuration. Future research directions include: (1) investigating the integration of wind, solar, and other renewable energy sources with energy storage systems to optimize overall power quality and operational efficiency in multi-energy systems;

(2) developing more efficient energy management strategies and equipment optimization models to extend the lifespan of energy storage devices while considering the impact of frequent harmonic suppression; (3) exploring optimization algorithms in complex, multi-objective environments to address high-dimensional and real-time dynamic power quality optimization challenges; and (4) comprehensively evaluating the environmental and economic benefits of energy storage systems to provide multi-dimensional decision support for energy storage equipment deployment.

Acknowledgement: Sincere thanks are due to Professor Caifeng Wen of Inner Mongolia University of Technology for providing lots of constructive suggestions.

Funding Statement: This research was funded by: the Inner Mongolia Nature Foundation Project, Project number: 2023JQ04.

Author Contributions: The contributions to this paper are as follows: research idea and design: Jian Gao, Caifeng Wen; data collection: Hongliang Hao, Yongsheng Wang, Yuwen Zhang; results analysis and interpretation: Jian Gao, Zhanhua Han, Edwin E. Nyakilla; first draft: Jian Gao, Caifeng Wen. All authors reviewed the results and approved the final version of the manuscript.

Availability of Data and Materials: Data is available on request from the authors. The data that support the findings of this study are available from the corresponding author, upon reasonable request.

Ethics Approval: Not applicable.

Conflicts of Interest: The authors declare no conflicts of interest to report regarding the present study.

Nomenclature

PSD	Power spectral density (W/Hz)
RMS	Root mean square
THDi	Total harmonic distortion rate of current
d_{RMS}	Effective value of voltage fluctuation
$\cos\varphi$	Power factor
N	Signal sequence length
Δt	Sampling interval (s)
Fs	Sampling frequency (Hz)
$\|x\|$	Amplitude after discrete Fourier transform
Δf	Sample frequency (Hz)
$X_i^*(f)$	Complex conjugate of the frequency domain signal
$S_w(f)$	PSD of wind power fluctuation
σ_y^2	Variance of the system frequency deviation PSD
T	System time inertia constant
β	Load-frequency characteristic coefficient
I_1	Effective value of fundamental current (A)
I_n	RMS of the n-th harmonic current (A)
$PSD(I_1)$	PSD corresponding to the effective fundamental current
$PSD(I_n)$	PSD corresponding to the n-th effective harmonic current
$\cos\varphi_1$	Fundamental power factor
m	Relative amplitude of interharmonics
f_i	Fundamental frequency (Hz)
f_{iH}	Interharmonic frequency (Hz)
Δf_i	Deviation between f_{iH} and f_i (Hz)

θ_{iH}	Phase angle
T_0	Fundamental period
V_1	Fundamental voltage amplitude (V)
V_n	n-th interharmonic voltage amplitude (V)
λ	Tip speed ratio
FFT	Fast Fourier transform
AR	Modern power spectrum estimation—autoregressive model
GA + Pareto	Genetic Algorithm + Pareto frontier search
NSGA-II	Non-dominated Sorting Genetic Algorithm-II
MOEA/D	Multi-Objective Evolutionary Algorithm Based on Decomposition

References

1. Mahdavi N, Mojaver P, Khalilarya S. Multi-objective optimization of power, CO_2 emission and exergy efficiency of a novel solar-assisted CCHP system using RSM and TOPSIS coupled method. Renew Energy. 2022;185(1–2):506–24. doi:10.1016/j.renene.2021.12.078.
2. Mojaver P, Khalilarya S, Chitsaz A. Combined systems based on OSOFC/HSOFC: comparative analysis and multi-objective optimization of power and emission. Int J Energy Res. 2021;45(4):5449–69. doi:10.1002/er.6173.
3. Tan L, Dong X, Gong Z, Wang M. Investigation on performance of an integrated SOFC-GE-KC power generation system using gaseous fuel from biomass gasification. Renew Energy. 2017;107(7):448–61. doi:10.1016/j.renene.2017.02.012.
4. Al-Qadri AA, Ahmed U, Ahmad N, Abdul Jameel AG, Zahid U, Naqvi SR. A review of hydrogen generation through gasification and pyrolysis of waste plastic and tires: opportunities and challenges. Int J Hydrog Energy. 2024;77:1185–204. doi:10.1016/j.ijhydene.2024.06.207.
5. Lalhmachhuana R, Deb S, Datta S, Singh KR, Cali U, Ustun TS. Multi-objective-based economic and emission dispatch with integration of wind energy sources using different optimization algorithms. Front Energy Res. 2024;12:1421212. doi:10.3389/fenrg.2024.1421212.
6. Xie M, Yan Y, Ke S, Liu M. Vector ordinal optimization theory based large-scale multi-objective unit commitment considering stochastic wind power. IEEJ Trans Electr Electr Eng. 2018;13(3):463–71. doi:10.1002/tee.22589.
7. Arshad M, Beik O, Manzoor MO, Gholamian M. Stability analysis *via* impedance modelling of a real-world wind generation system with AC collector and LCC-based HVDC transmission grid. Electronics. 2024;13(10):1917. doi:10.3390/electronics13101917.
8. Elenets MV, Nemirovich-Danchenko MM. Application of the Prony method for biometric data analysis. J Phys: Conf Ser. 2021;1862(1):012007. doi:10.1088/1742-6596/1862/1/012007.
9. Xu Y, Fan SS, Xie S, Lu M. Power quality dectection and classification in active distribution networks based on improved empiricial wavelet transform and disperson entropy. CSEE J Power Energy Syst. 2020;8(6):1646–58.
10. Leonowicz Z, Lobos T. Power quality evaluation using advanced spectrum estimation methods. In: 2006 International Conference on Power System Technology; 2006 Oct 22–26; Chongqing, China. p. 1–6. doi:10.1109/ICPST.2006.321955.
11. Wang N, Sun M, Xi X. Identification of power quality disturbance characteristic based on deep learning. Electr Power Syst Res. 2024;226(3):109897. doi:10.1016/j.epsr.2023.109897.
12. Narendra Babu P. Adaptive grid-connected inverter control schemes for power quality enrichment in microgrid systems: past, present, and future perspectives. Electr Power Syst Res. 2024;230(3):110288. doi:10.1016/j.epsr.2024.110288.
13. Shao H, Henriques R, Morais H, Tedeschi E. Power quality monitoring in electric grid integrating offshore wind energy: A review. Renew Sustain Energy Rev. 2024;191:114094. doi:10.1016/j.rser.2023.114094.
14. Hołdyński G, Skibko Z, Firlit A, Walendziuk W. Analysis of the impact of a photovoltaic farm on selected parameters of power quality in a medium-voltage power grid. Energies. 2024;17(3):623. doi:10.3390/en17030623.
15. Tian Z. Analysis and research on chaotic dynamics behaviour of wind power time series at different time scales. J Ambient Intell Humaniz Comput. 2023;14(2):897–921. doi:10.1007/s12652-021-03343-1.

16. Yao L, Wang W, Cai W, Liu J. Storage size determination for grid-connected wind power system based on power spectral density analysis. J Clean Prod. 2021;325(2):129247. doi:10.1016/j.jclepro.2021.129247.
17. Qing X, He W, Zhou M, Du W. Quantifying fluctuations for dynamical power systems with stochastic excitations: a power spectral density-based method. Chaos. 2023;33(5):053113. doi:10.1063/5.0147018.
18. Ayon JJ, Barocio E, Cabrera IR, Betancourt R. Identification of coherent areas using a power spectral density algorithm. Electr Eng. 2018;100(2):1009–19. doi:10.1007/s00202-017-0564-9.
19. Nasab MA, Al-Shibli WK, Zand M, Ehsan-maleki B, Padmanaban S. Charging management of electric vehicles with the presence of renewable resources. Renew Energy Focus. 2024;48(3):100536. doi:10.1016/j.ref.2023.100536.
20. Azimi Nasab M, Ali Dashtaki M, Ehsanmaleki B, Zand M, Azimi Nasab M, Sanjeevikumar P. LFC of smart, interconnected power system in the presence of renewable energy sources using coordinated control design of hybrid electric vehicles. Renew Energy Focus. 2024;50(1):100609. doi:10.1016/j.ref.2024.100609.
21. Karafotis PA, Georgilakis PS. Power quality monitoring and evaluation in power systems under non-stationary conditions using wavelet packet transform. High Volt. 2019;4(3):186–96. doi:10.1049/hve.2019.0062.
22. Chen Y, Tang Z, Weng X, He M, Zhang G, Yuan D, et al. A novel approach for evaluating power quality in distributed power distribution networks using AHP and S-transform. Energies. 2024;17(2):411. doi:10.3390/en17020411.
23. Karakaya O, Balci ME, Hocaoglu MH. Minimization of voltage harmonic distortion of synchronous generators under non-linear loading via modulated field current. Energies. 2023;16(4):1789. doi:10.3390/en16041789.
24. Merabet Boulouiha H, Khodja M, Rahiel D, Allali A, Kaddour F, Denaï M. Power quality enhancement in electricity grids with wind energy using multicell converters and energy storage. J Renew Sustain Energy. 2019;11(1):013302. doi:10.1063/1.5043292.
25. Guo Y, Wang Q, Zhang D, Yu D, Yu J. A stochastic-process-based method for assessing frequency regulation ability of power systems with wind power fluctuations. J Environ Inform. 2018;32(1):45–54. doi:10.3808/jei.201800394.
26. Lin BR, Hou YL, Chiang HK. Implementation of a three-level rectifier for power factor correction. IEEE Trans Power Electron. 2000;15(5):891–900. doi:10.1109/63.867678.
27. Tayjasanant T, Wang W, Li C, Xu W. Interharmonic-flicker curves. IEEE Trans Power Deliv. 2005;20(2):1017–24. doi:10.1109/TPWRD.2004.838639.
28. Wen C, Zhang B, Dai Y, Wang W, Xie W, Du Q. The correlation between the power quality indicators and entropy production characteristics of wind power + energy storage systems. Energy Eng. 2024;121(10):2961–79. doi:10.32604/ee.2024.041677.
29. Wen C, Wang Q, Cao Y, Zhang L, Wang W, Zhang B, et al. Correlation analysis of wind turbine temperature rise and exergy efficiency based on field-path coupling. Energy Eng. 2023;120(7):1603–19. doi:10.32604/ee.2023.027074.
30. Hong X, Tian L, Yin X, Xu M, Han L, Liu X. Influence of large-scale distributed photovoltaic access on harmonic characteristics of distribution network. J Phys: Conf Ser. 2023;2592(1):012076. doi:10.1088/1742-6596/2592/1/012076.
31. García H, Segundo J, Madrigal M. Harmonic analysis of power systems including thyristor-controlled series capacitor (TCSC) and its interaction with the transmission line. Electr Power Syst Res. 2014;106(3):151–9. doi:10.1016/j.epsr.2013.08.013.
32. Zhang Y, Sun H, Tan J, Li Z, Hou W, Guo Y. Capacity configuration optimization of multi-energy system integrating wind turbine/photovoltaic/hydrogen/battery. Energy. 2022;252(7):124046. doi:10.1016/j.energy.2022.124046.
33. Spunei E, Piroi I, Protea B, Piroi F. The power factor and the upper harmonics. J Phys: Conf Ser. 2021;1781(1):012037. doi:10.1088/1742-6596/1781/1/012037.